



Research article

Evaluation of AVIRIS-NG hyperspectral images for mineral identification and mapping

Mahesh Kumar Tripathi ^{*}, H. Govil*National Institute of Technology, Raipur, Chhattisgarh, India*

ARTICLE INFO

Keywords:
 AVIRIS-NG
 Hydrothermal alteration
 Remote sensing
 Clay minerals
 Western Jhajhpur belt
 Geology
 Bhilwara

ABSTRACT

Advancement of airborne hyperspectral remote sensing techniques provides subtle variations to identify minerals and to make distinctions between rock formations. These techniques clearly define barren land versus economically viable zones containing ores and minerals. As we know profitable mineral zones are commonly associated with hydrothermal alteration zones, hyperspectral remote sensing techniques have the capability to identify and distinguish between altered, weathered, and clay minerals. In this research work, airborne hyperspectral remote sensing image from AVIRIS-NG is used to identify hydrothermally altered minerals in the Jhajhpur region of Bhilwara district, Rajasthan, India. The purpose of this study is the identification of the minerals through spectral features of image spectra in corroboration with field sample spectra and USGS laboratory spectra. The spectral angle mapper (SAM) and Spectral Feature Fitting (SFF) algorithms were used for the mapping of the minerals. This study was conducted to prove the capability of AVIRIS-NG hyperspectral remote sensing data to identify zones of profitable mineral deposits.

1. Introduction

Since the inception, remote sensing techniques playing valuable and significant contributions in the field of geology and mineral exploration [1]. The combination of remote sensing and spectroscopy is known as imaging spectroscopy or hyperspectral remote sensing [2]. Since the time of evolution, the imaging spectroscopy has become more significant in identification, discrimination, and mapping of the earth surface features due to their chemical composition and structures [3]. Last three decades of progressive development of hyperspectral remote sensing have provided some spaceborne and airborne hyperspectral sensors such as airborne imaging spectrometer (AIS), advanced visible infrared imaging spectrometer (AVIRIS), Hyperspectral Digital Imagery Collection Experiment (HYDICE), digital airborne imaging spectrometer (DAIS), Hyper-spectral Mapper (HYMAP) and Hyperion for lithological discrimination, mineral identification and mapping [2, 4, 5, 6, 7].

The advent of hyperspectral sensor allows us to map/identify the qualitative surface minerals such as clay group of minerals kaolinite, montmorillonite) talc, muscovite, iron hydroxides/oxides (hematite, goethite, magnetite), sulfate minerals (alunite), carbonate minerals (calcite, dolomite), and silica (quartz) etc. through spectral features. These spectral features are also known as the signature curve of objects or

minerals [1, 8]. Mapping of these minerals allowed identification of different alteration facies (propylitic, argillic, advanced argillic, etc.); [6, 7, 9, 10].

Widely, two major spectral intervals are used in the range of 0.4–2.5 μm of the electromagnetic spectrum (EMR) for geological applications such as mineral identification and lithological mapping [10, 11, 12, 13, 14, 15, 16]. There are several applications of hyperspectral remote sensing data. According to Kruse (2003) advanced visible infrared imaging spectrometer (AVIRIS) has wide applications in mineral mapping such as hydrothermal alterations and developing expert system (linear spectral unmixing method (buddingtonite mineral bound ammonium in hydrothermally altered volcanic rocks in the southern Cedar Mountains [11]), spectral angle mapper and tricorder algorithms (mapping kaolinite group of minerals and ferric oxides) [6, 12, 13]. The spectral data extracted from AVIRIS broadly used as a proxy to identify and map the specific minerals on the behalf of diagnostic absorption feature which depend upon the quantitative relation between absorption depth and concentration of mineral phase such as, primary rock-forming minerals and secondary alteration, weathering products [11].

The Hyperion (242 bands) and AVIRIS (224 bands) sensor had some drawbacks such as low signal to noise ratio, striping and geometric distortions such as smile and keystone errors [14]. In the detailed and more

* Corresponding author.

E-mail address: tripathi.mahesh1@gmail.com (M.K. Tripathi).

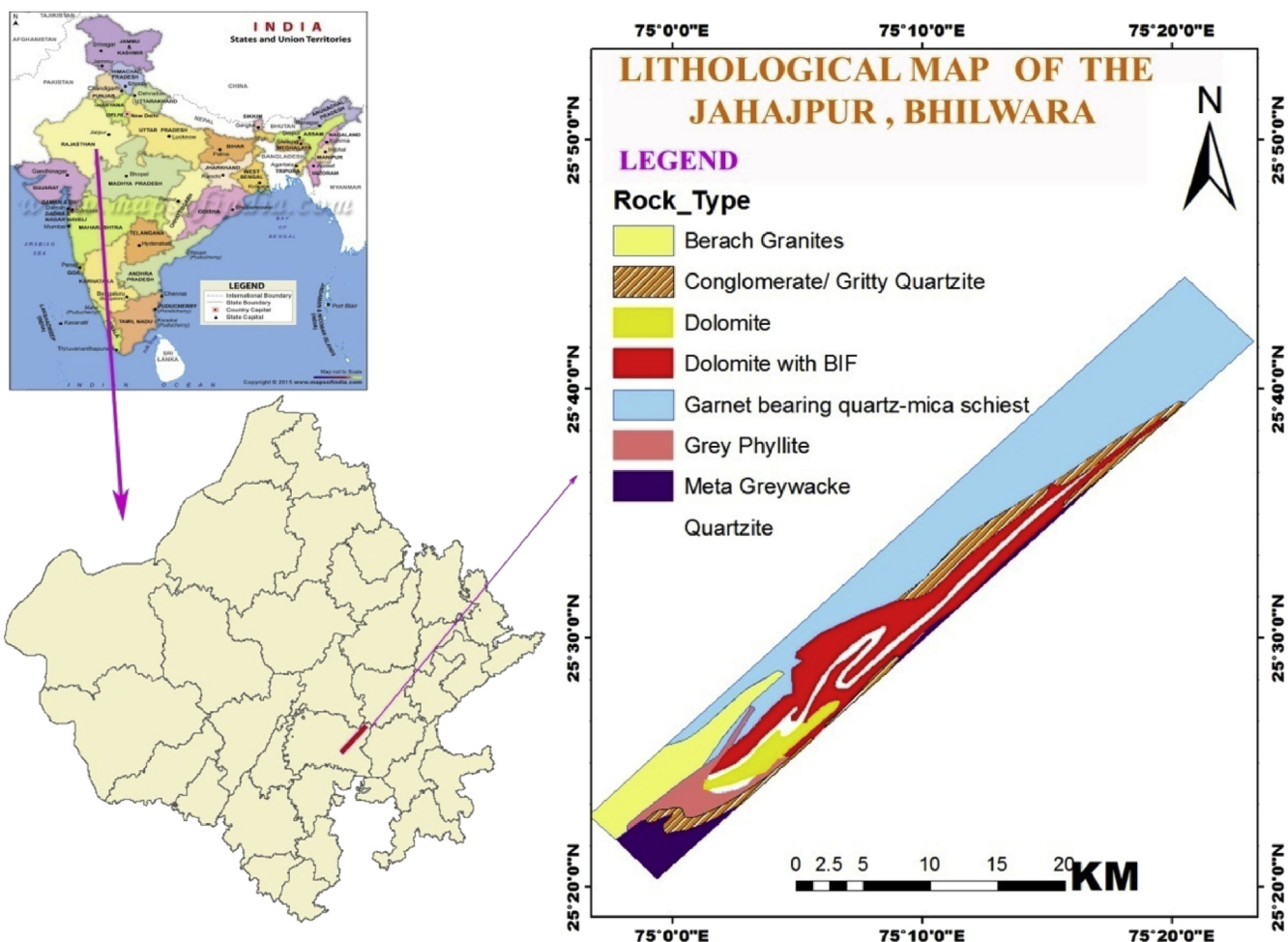


Figure 1. Geology map of the study area [17, 18, 19]

specific study Jet propulsion laboratory, National aeronautics and space administration (JPL NASA) had planned to develop new advance airborne sensor AVIRIS- NG with several specifications which make it more significant for identification, discrimination and mapping [6, 7, 15, 16, 17].

On 04 February 2016, a joint mission of Indian space research organization (ISRO) and NASA airborne hyperspectral remote sensor (AVIRIS-NG) had executed mission flights to capture images for mineral mapping and identification in Jahajpur, India. AVIRIS-NG, a new airborne hyperspectral sensor, has 425 spectral bands with high spatial and spectral resolution in $0.4\mu\text{m}$ – $2.5\mu\text{m}$ spectral range. In recent trends of airborne systems of hyperspectral remote sensing AVIRIS-NG can be considered as the most advance data for mineral identification and mapping [6, 7].

2. Geological settings

Jahajpur is located in Bhilwara, Rajasthan, India (25.62°N 75.28°E ; Figure 1). It has an average elevation of 334 m (1095 feet). The study

area region of Bhilwara supergroup belongs north western shield of Archean age [20]. Jahajpur Group of Bhilwara Supergroup occupies the major part of the Jahajpur area. The Jahajpur region is associated with three different geologic age groups of rocks such as the Mangalwar complex, the Hindoli group and the Jahajpur group [20]. The major rock types in the area are dolomite, phyllite, and quartzite [21]. The abundant minerals in the study area are clay, talc, iron, and talc. Occurrences of soapstone in dolomitic limestone/quartzite belong to Pre-Aravali. In the Jahajpur area two parallel ridges of dolomitic limestone occur from Ghevaria (SW) up to Jahajpur (NW) [6, 7].

3. Data and methodology

AVIRIS-NG data was acquired in February 2016 for the study area. AVIRIS-NG is a hyperspectral imaging spectrometer with 427 contiguously spaced 5nm bands from 0.38 to $2.51\mu\text{m}$ and 8.1m spatial resolution [14, 23]. AVIRIS-NG hyperspectral data parameters are given in Table 1. AVIRIS-NG data is “free from keystone and smile error distortions” [14]. The adopted methodology is divided into two parts such as identification and mapping. Before identification and mapping, there are some initial steps are involved for image preprocessing and atmospheric correction. There are some necessary steps in image preprocessing which are pre-image calibration, band removal, atmospheric correction, and dark subtraction methods. The extracted image spectra from AVIRIS-NG verified with the resampled USGS spectral library and field sample spectra. The next step is identification and discrimination of minerals absorption and reflectance for particular mineral at a particular bandwidth through visual image interpretation. AVIRIS-NG derived spectral

Table 1. Specification of AVIRIS-NG [14, 15, 24]

Sensor Altitude	4–8 km	Spectral Range	0.380 – $2.510\mu\text{m}$
Spatial Resolution	8.1 m	Spectral Coverage	Continuous
Swath Width	4 – 6 km	Spectral Resolution	$5\text{nm} \pm 0.5\text{ nm}$
VNIR Range	400nm – 1000nm	SWIR range	0.900 – $2.500\mu\text{m}$
IFOV (mrad)	1.0 mrad	Total number of bands	425

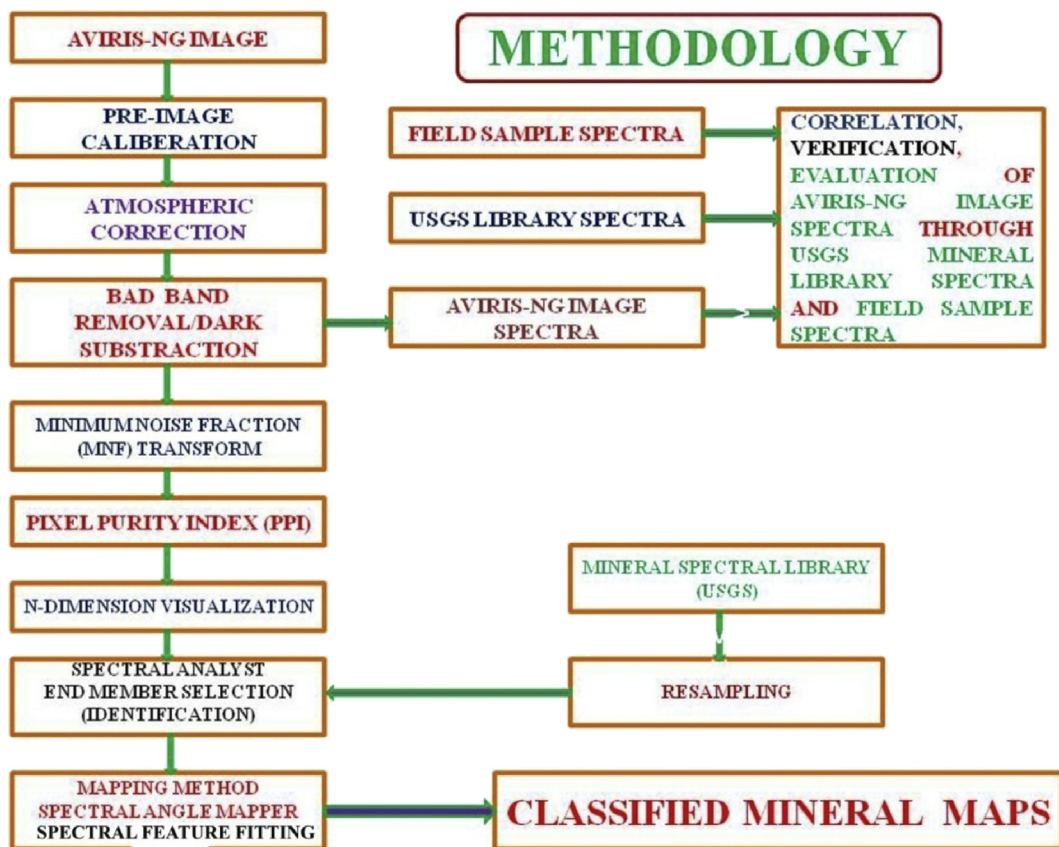


Figure 2. Flow diagram of the methodology.

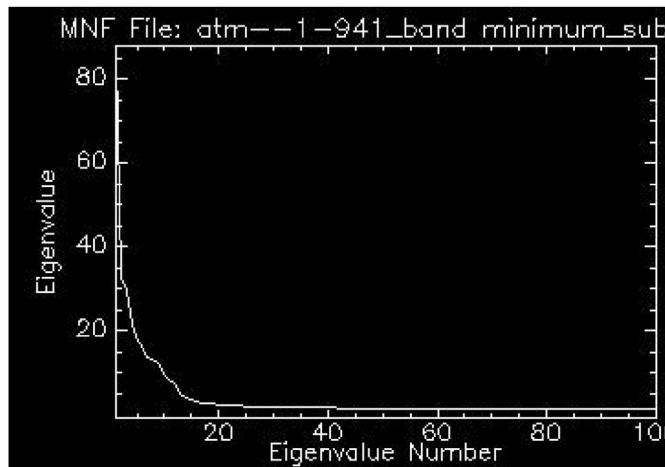


Figure 3. MNF Eigen value graph.

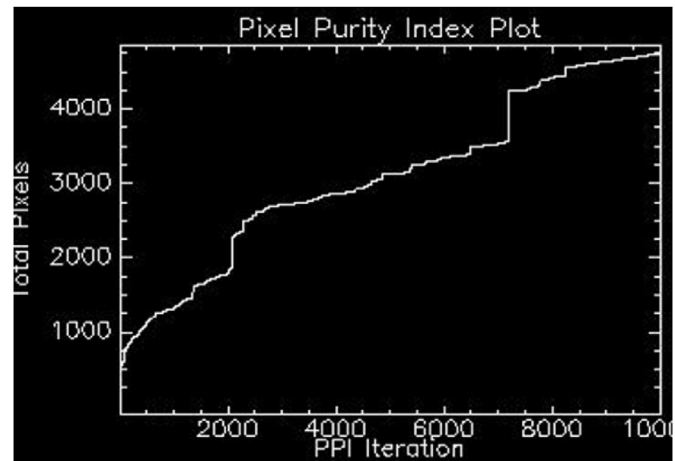


Figure 4. Pixel purity index plot.

signatures were also matched with USGS spectral library and field sample spectroscopic analysis for the evaluation of minerals [23].

In the process of mineral mapping, there are some steps involved which have shown in the flow diagram of methodology. Systematic patterns to processing the AVIRIS-NG data for the mineral mapping are given below. The detailed methodology flowchart is given in (Figure 2).

3.1. Preprocessing of AVIRIS-NG data

A large number of narrow and contiguous bands cause radiometric errors in the hyperspectral data. So the correction of the image requires pre-image processing of satellite data. Available data set has been used in

raw form. Acquired data from the agency are radiometrically, geometrically and atmospherically uncorrected. Due to the atmospheric effect data set is included with some errors. So, there is a requirement for atmospheric correction and radiometric calibration. AVIRIS-NG data set is away from the smile effect because AVIRIS-NG has a higher signal to noise ratio [14, 15, 16, 17, 24].

3.2. Atmospheric correction

Remote sensing sensor captures the radiance energy which passes from sun to earth surface and earth to sensor through the atmosphere of the earth. To get true reflectance energy of the object of earth surface

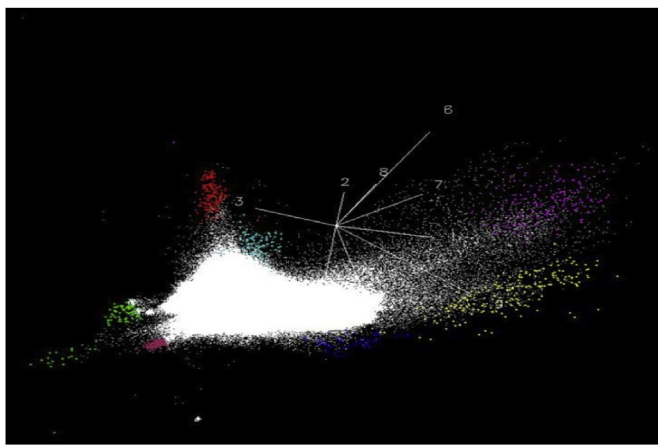


Figure 5. N-D visualization image.

requires some necessary atmospheric coefficients for atmospheric correction. To get ground reflectance the atmospheric coefficients require compensation such as surface altitude, surface albedo, aerosol, water vapor column, surface, and atmospheric temperatures, cloud optical depths, scene-visibility. In the process of atmospheric correction estimation of water vapor calculated pixel by pixel independently in AVIRIS-NG image [25, 26]. The FLAASH model applied for removal of haze, noise, atmospheric influences on the radiance image of AVIRIS-NG image from visible to shortwave infrared.

3.3. FLAASH

FLAASH model works on a standard equation on flat, Lambertian materials for spectral radiance at a sensor pixel, L. The equation is given as –

$$L = \left(\frac{A\rho}{1 - \rho e S} \right) + \left(\frac{B\rho e}{1 - \rho e S} \right) + L_a \quad (1)$$

Where- ρ - Pixel surface reflectance; ρe -Radiance at sensor's-Atmospheric spherical albedo; L_a -Backscattered radiance by atmosphere; A & B are coefficients(depend upon atmospheric and geometric condition) [26].

3.4. MNF transformation

The hyperspectral imagery has huge data volume (data dimensionality) which causes the maximum data processing and higher complex computation. MNF transform higher data dimensionality into low dimensionality of data without losing the information. To segregate the random noise and reliable estimation of data dimensionality from the signal information.

The MNF transformation method was developed by Green et al., (1988) for dimensionality reduction and qualitative analyses of the image in form transformation of image components in a significant order [27]. The whitening image has not any band to band correlations. The whitening image has unit variance. The decorrelation and rescaling of noise is the result of whitening image. The first PC transform is focused on the whitening noise of data. The second standard PC transform provide arranged and non-correlated information in terms of decreasing content (noise). The lesser eigen values than 1 in MNF components

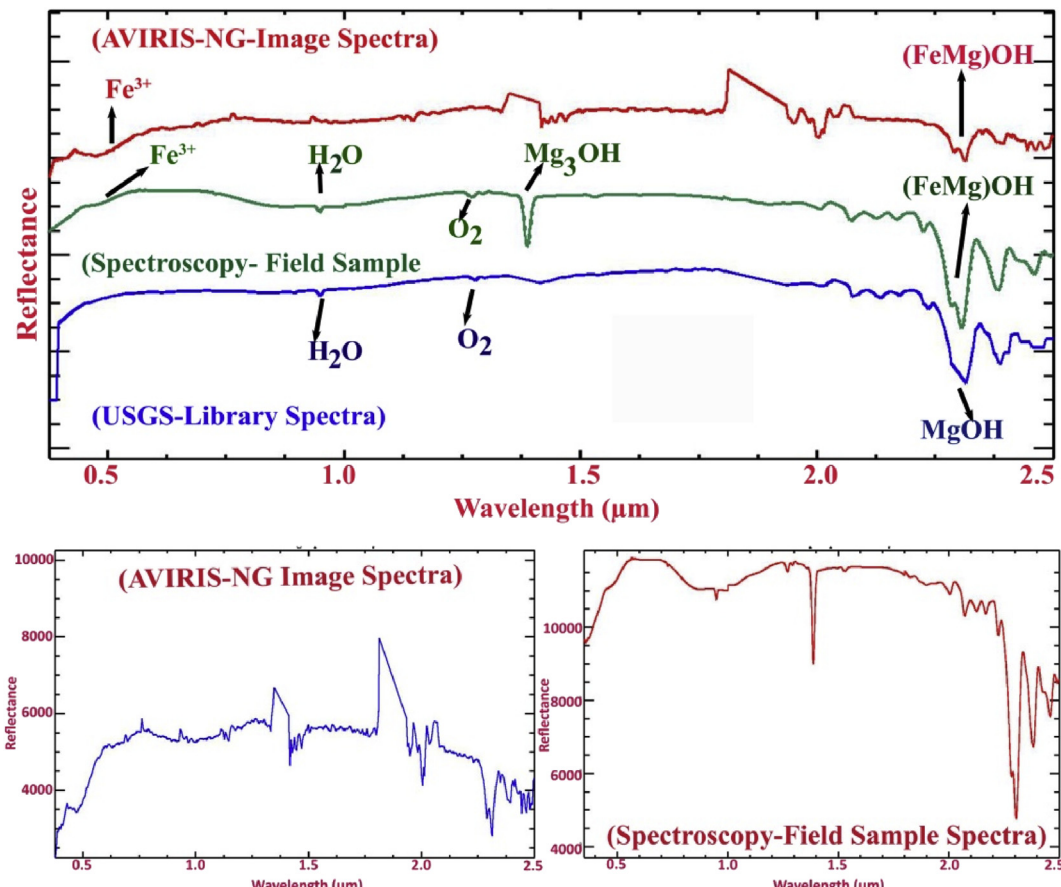


Figure 6. Spectral plots of minerals Talc.



Figure 7. Field photographs of minerals locations: A) Goethite mineral deposits at Itawa, B) Montmorillonite mineral deposits at Itawa, C) Talc mineral deposits at Chainpura, D) Kaolinite mineral deposits at Chhabadiya, E) Talc mineral Deposits at Gheoriya, F) Goethite/Limonite deposits at Omkarpura, G) Kaolinite mineral deposits at Omkarpura, H) Montmorillonite deposits at Omkarpura, I) Goethite deposits at Kanti, J) Kaolinite and Talc deposits at Ummepura, K) Kaolinite mineral deposits at Ampura, L) Goethite deposits at Itwa, M) Dolomite limestone deposits at Kanti, N) Goethite deposits at Meera Nagar, O) Goethite mineral deposits at Bonai Kheda and P) Kaolinite deposits at Rampura.

usually excluded from noise data and which eigen values are the near value of 1 in MNF are normally noise dominated [28]. This is not a mineral mapping method but variations in MNF color assignments provide an explanation as variation in mineral composition or abundance [29]. The MNF approach applied to AVIRIS-NG data set to get reliable information. The MNF eigen value graph has shown in (Figure 3).

3.5. End member extraction

In AVIRIS-NG data set extraction of spectral end members in specific and favorable regions are possible through combine approach of MNF, PPI, and n-d visualization. According to Meer (2012), the PPI is significant statistical technique to get pure pixels [30]. The pixel purity index is an automated tool for end member extraction through the MNF image. The automatic determination of relative pure pixels from high values of MNF Eigen image through convex geometry called as pixel purity index. Determination of pixel purity index is possible through multiple repeated projections of n-d scatter plots on the behalf of random unit vectors. Extreme pixels are more frequently recorded because they have higher relative purity according to the brightness of pixels in the PPI image [31]. For analysis of end member determination, by default scatter plot of 10, 000 projections and 2.5 threshold factor applied on to the MNF band image to reduce the purer materials from mixed and to select the purest PPI pixels (Figure 4).

Extraction of purest pixels spectra through the spectral mixing space n-dimension visualization is more significant and interactive techniques in image classification [32]. The scattering points (pixels) in n-dimension

visualize scatter plot consider as spectra in which 'n' is denoted as the number of bands. The points (pixels) spin in real time in the n-d scatter plot (Figure 5). In n-d visualization for a single band, each pixel has n values and coordinates in n-space. The estimation of extremely pure pixels or end members through the point's distribution in the n-d space [33]. The selection of the region of interest (ROI) is based on the n-dimensional visualization process for the selection of extreme pixels or those pixels which have the highest pixel. Extraction of pure pixel and determination of their spectra, the n-dimensional visualization method applied to ROI on MNF image. These spectra derived from FLAASH calibrated images. Using USGS reference mineral spectral library matching all spectra collected to mineral zones [31, 34].

3.6. Spectral angle mapper

SAM algorithms applied for identification of minerals which is based on the measurement of similarity between the reference spectra and image spectra through the calculation of spectral angle between two vectors having the same origin. Calculation of length of a spectrum vector ($L\rho$) as

$$L\rho = \sqrt{\sum_{i=1}^N \rho_i^2} \quad (2)$$

Similarity determination of an unknown spectra x to a reference spectrum y through SAM algorithms by this equation

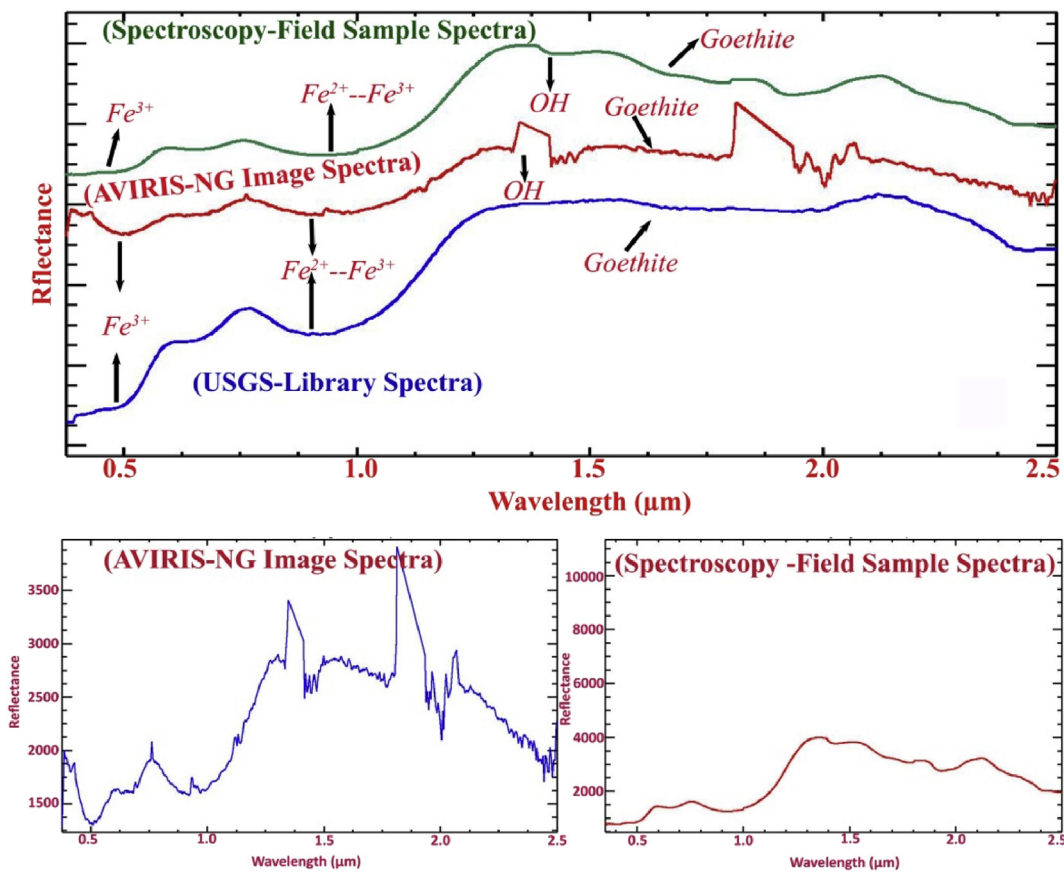


Figure 8. Spectral plots of minerals Goethite.

$$\theta = \cos^{-1} \left(\frac{\sum_{i=1}^M \rho_i \rho'_i}{L\rho L\rho'} \right) \quad (3)$$

3.7. *Lρ*-length of the end member vector

Lρ-Length of the modeled spectrum vector [35, 36]

Classification of spectrum depends on the class of end member when the modeled spectrum angle is below the threshold determined by the user. The initial advantage of the SAM spectral angle is insensitive to differentiate the albedo of the modeled spectrum. Length of each vector measured by spectral albedo and spectral shape difference measured in spectral angles [9, 37, 38].

3.8. Spectral feature fittings (SFF)

The principle of spectral feature fittings method is based on the elimination of continuum of absorption features by reference spectra and each image spectra [39]. In the process of least square fitting operation of spectral feature fittings method, there is a comparison among continuum removed image spectra and continuum reference spectra [36]. The most significant spectra of fitted materials selected on the basis of correlation coefficients through the process of division of each original image pixel spectrum (S) and (C) continuum curve which have shown in the equation [40]-

" $\text{Scr} = S/C$ (4)"

Where Scr = Continuum-removed spectra, S = Original spectra, C = Continuum curve.

There are some steps involved in SFF such as Scale Image and Root Mean Square (RMS) error image. The generation of scale images started by subtraction of the continuum removed spectra by one. Scale image

provides information for prediction, measurement of the depth of the absorption feature in each pixel. The abundance of spectral features represented by scale factor by calculation of band to band through the computation of least-square fit process. The higher scale factor value related to strong absorptions of minerals [39]. The brightness of scale image is an indication of better matching of the image spectrum to the reference spectrum of minerals in pixel. The root mean square error (RMSE) image pixels appearing darker and shape of spectra more similar to reference spectra of minerals. This is used for the existence and absence of minerals. There is the interrelationship between scale image and RMSE image is that low RMSE and high scale factor value indication of highly or closely matching of minerals. There is a condition scale image and RMSE image quantity will be equal.

4. Result and discussion

At the location of Ghevaria village, image spectra of talc minerals have shown different diagnostic absorption features at $2.31\mu\text{m}$ with doublet at $2.28\mu\text{m}$ due to vibrational absorption features of Mg-OH and absorption found at $2.0\mu\text{m}$ and $2.37\mu\text{m}$ - $2.38\mu\text{m}$ due to the combination of dolomite and overtones bands of CO_3 , O_3 , and H_2O respectively. Field sample spectra of the minerals of Ghevaria have distinct absorption features at $2.30\mu\text{m}$ with doublet $2.28\mu\text{m}$ (Figure 6).

The goethite ($\text{Fe}^{+3}\text{O(OH)}$) minerals are found in Omkarpura, Itwa, Kanti, and Meera Nagar (Figure 7). The goethite minerals are found in dolomitic rocks of the study area. The image spectra have absorption at 0.54 , $0.92\mu\text{m}$ due to electronic absorption. Spectral interpretation details of field samples of goethite are similar to image spectra on major absorption feature at $0.50\mu\text{m}$, $0.62\mu\text{m}$, $0.93\mu\text{m}$, $1.41\mu\text{m}$, $1.80\mu\text{m}$ (Figure 8).

The montmorillonite minerals identified in Chhabadiya, Itwa, and Omkarpura (Figure 7) through distinct absorption features at $2.20\mu\text{m}$

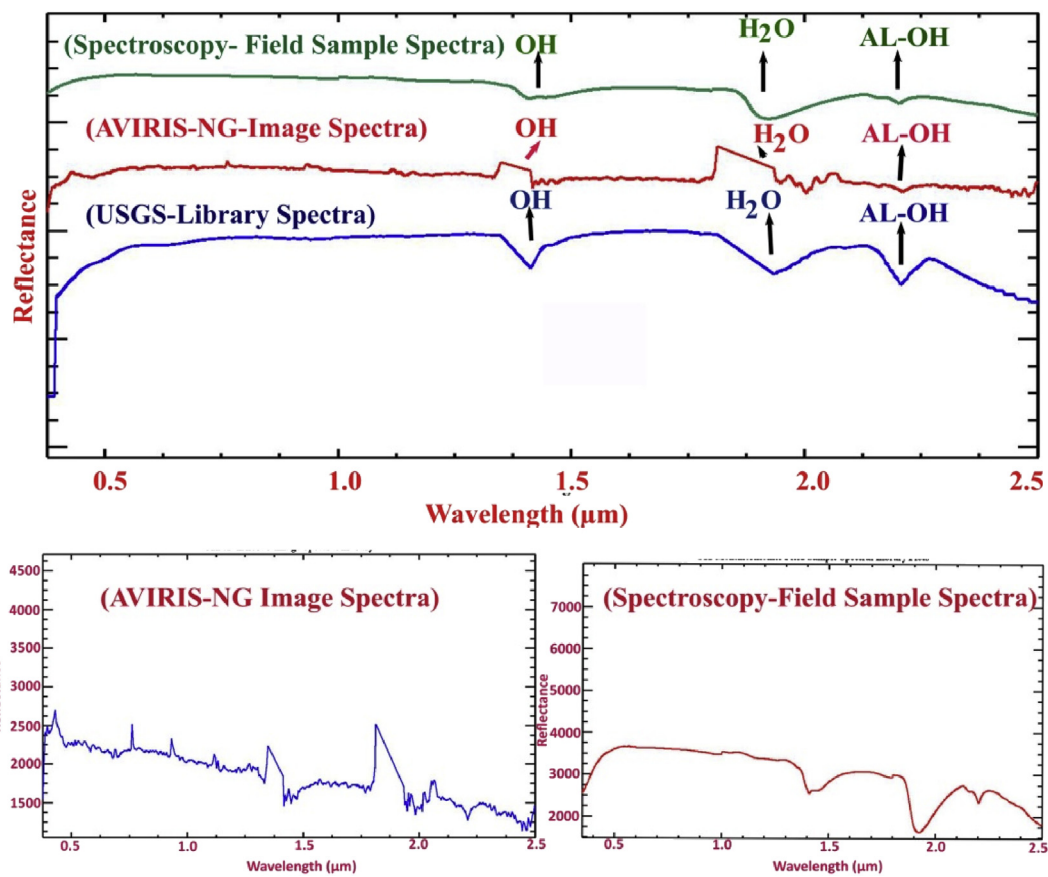


Figure 9. Spectral plots of minerals Montmorillonite.

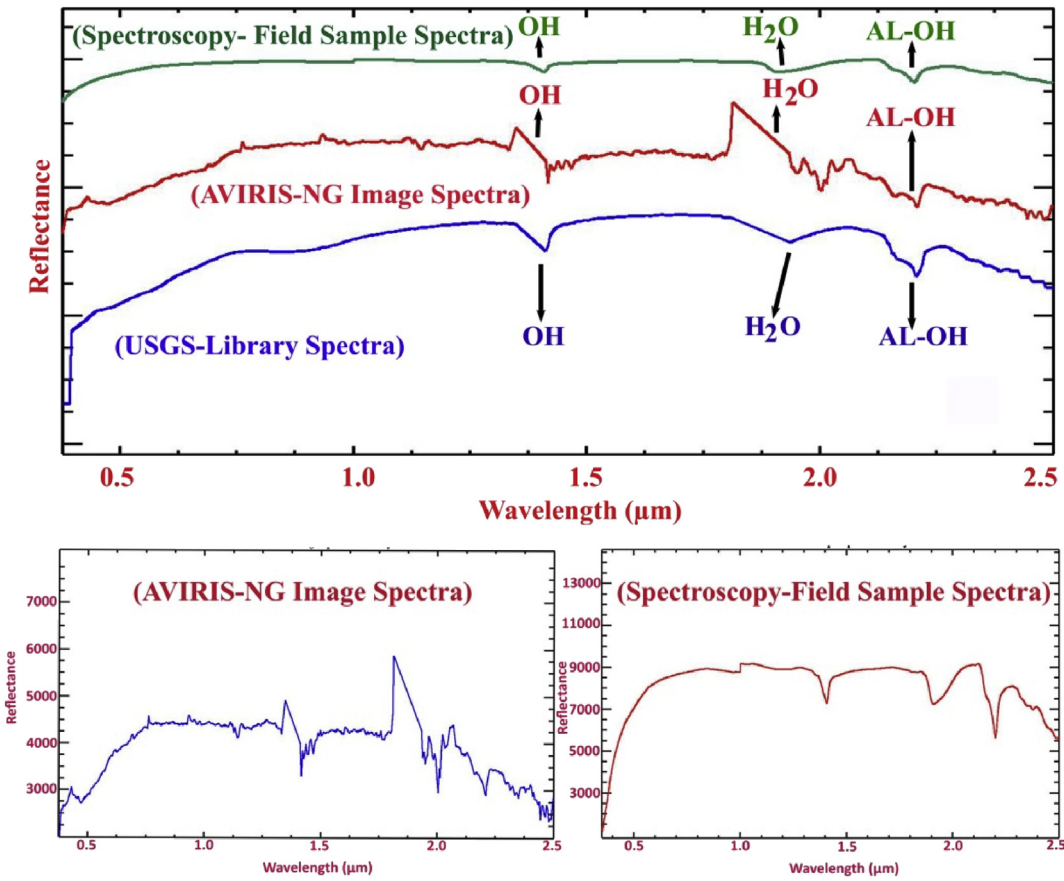


Figure 10. Spectral plots of minerals Kaosmec.

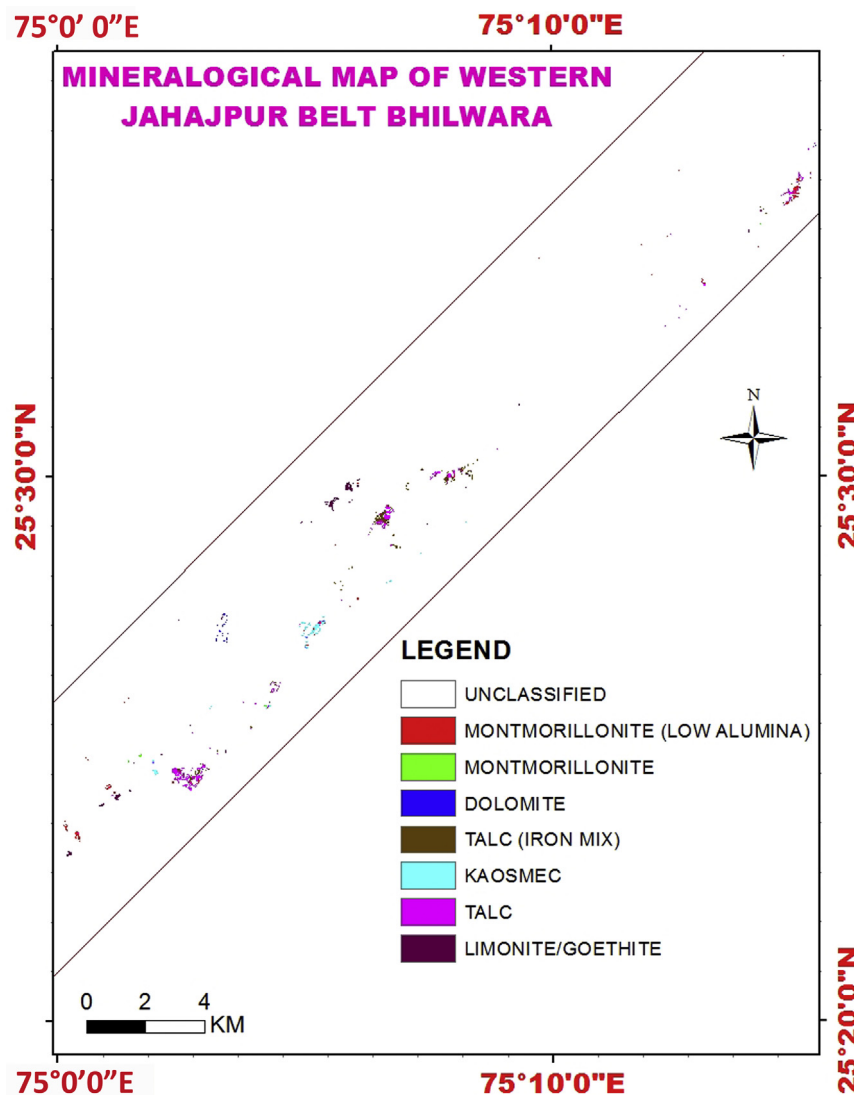


Figure 11. Mineral distribution map of Jahajpur region India.

due to the presence of Al-OH. In field spectra major absorption due to Al-OH at 2.20 μm . The kaosmec (Kaolinite-Smectite) minerals identified in Madhopur, Barenkheda, and near Ghevaria village through distinct absorption features at 2.20 μm and 2.15 μm due to Al-O H. In field sample spectral absorption due to the presence of Al-OH at 2.20 μm and 2.15 μm . Sharp absorption features at 1.41 μm , 1.94 μm due to the OH stretching and H-O-H overtones in image spectra of limonite/goethite, talc, montmorillonite, kaosmec respectively. Identified minerals in the study area are talc, montmorillonite, kaosmec, which shows strong absorption features at 2.3 μm , 2.2 μm respectively [41] and the absorption features around at 0.5 μm , 0.65 μm and 0.9 μm are typical of goethite [42] (Figures 9 and 10).

In the analysis for interpretation for preparation of mineral maps 390 out of 425 bands are selected for further hyperspectral image processing for the conversion of radiance to reflectance image and for resizing the data 100 bands selected from region of 0.38 μm -2.5 μm . The higher eigenvalues of MNF are an indicator of the highest information available with the dimensionality of 10. The higher information probability in initial MNF bands and the rest number of band contained with noise. Here absorption features identified in the region of 0.45 μm , 0.92 μm , 1.3 μm , 1.4 μm , 1.80 μm , 1.93 μm , 2.1 μm , 2.2 μm , 2.31 μm and 2.39 μm . In the processed image there seven end members extracted such as limonite/goethite, talc, montmorillonite, kaosmec, and dolomite. Here two variety of montmorillonite and talc on the basis absorption and difference in

image spectra (due to iron inclusion) with respect to the USGS spectral library. The reflectance and absorption plot value of USGS resampled spectra library with respect to image spectra ranging from 0 to 10000 or 0–100 percent.

The study of SAM algorithm has chosen for surface composition mineral mapping, in which the USGS spectral library used as reference spectra to compare the similarity of the image spectra for mineral classification. SAM classification is used for the generation of maps of selected mineral on the maximum threshold value of SAM. The threshold values for talc, iron mix talc, montmorillonite which have low alumina content, montmorillonite, kaosmec, calcite, and limonite/goethite are 0.08, 0.07, 0.08, 0.05, 0.08, 0.09 and 0.08 radians. In the classified image red color denotes montmorillonite (low alumina) mineral, blue color for dolomites, green for montmorillonite, magenta for talc, yellow for iron mix talc and cyan for kaosmec and maroon for limonite/goethite (Figures 11 and 12).

In the study of mineral mapping, spectral feature fitting (SFF algorithms) method classified the same minerals. The classified minerals are interpreted and mapped at the default threshold (30 for all) values for all in scale image and RMSE image. The SFF has shown the potential to map different varieties of clay minerals such as kaolinite, montmorillonite, smectite, dolomite, and goethite. In the classified map, SFF has shown potential to map the minerals such as clay in river channel. The color symbology is the same as the SAM classification of minerals.



Figure 12. SAM and SFF algorithms method classified maps (AVIRIS-NG) of minerals in the study area.

5. Accuracy assessment

The interpreted results of mapping methods are validated to field surveys in the study area. The location of interpreted results and observed results validated with field sample spectra and USGS library spectra. All the observations of AVIRIS-NG image mineral classification matching accurately in the study area in observation of GPS survey and field photographs. The field photographs of identified minerals have shown in the figures such as listed below.

6. Conclusion

Clay group (montmorillonite, kaosmec, talc) and goethite identified through hyperspectral AVIRIS-NG remote sensing data, matched with spectroscopy measured spectral features of field samples and USGS spectral library spectra. In the result montmorillonite shows absorption at 2.2 with strong water bond absorption at 1.9 and weaker at 1.4 μm which is possibly better in the AVIRIS-NG image due to high S/N ratio and high spectral/spatial resolution. In talc and goethite mineral spectra absorption at 0.46, 0.76, 0.96, 2.0 and 2.39 μm which is indicating iron oxide/hydroxide and carbonate mineral association. The talc mineral image spectra and field sample spectra have shown the presence of some other minerals such as iron oxides (goethite) which indicates the capability and potential of AVIRIS-NG hyperspectral data. So, on the basis of identification of these mineral assemblages AVIRIS-NG data have the capability to map the alteration minerals because these minerals are an indicator of argillic alteration and gossanized product of oxidation and reduction, and weathering environment. It has a better response in the identification and determination of hydrothermally altered, weathered and clay minerals. Spectral signature for the studied field samples has shown an excellent similarity and agreement with spectral signature for AVIRIS-NG hyperspectral image.

The spectral angle mapper (SAM) algorithms applied for mineral mapping. Each mineral spectra have unique absorption value so, the minor variation in spectra identified in AVIRIS-NG image spectra such as the minor concentration of iron oxides in talc minerals. On the basis of various images spectral features, the minerals of western Jahajpur belt are in five major classes such as talc, montmorillonite, kaosmec, dolomite and limonite/goethite. The SFF method has also shown better results of minerals as SAM, but there is some variation in the distribution of minerals in the study area. SFF method provides minor to major mapping and classification capability and potential compare to SAM. In this research work it is found that high resolution hyperspectral data (AVIRIS-NG) have a better facility for detailed and comprehensive study of minerals. Extracted image spectra have higher reliability in mapping of clay and talc minerals, which prove the usefulness of better geologic information. The detection and mapping of alteration zone show the feasibility of AVIRIS-NG hyperspectral data in this study because the clay group of minerals is good for identification for alteration types. Including higher efficiency and accuracy AVIRIS-NG airborne hyperspectral remote sensing provide significant mineral maps in the study area.

These results are the demonstration of the usefulness of AVIRIS-NG hyperspectral data and the efficiency of the methods to the identification of remote minerals.

Declarations

Author contribution statement

Mahesh Kumar Tripathi: Conceived and designed the experiments; Performed the experiments; Analyzed and interpreted the data; Wrote the paper.

Himanshu Govil: Contributed reagents, materials, analysis tools or data.

Funding statement

This work was supported by Space Application Centre, Indian Space Research organisation India grant EPSA/4.2/2017.

Competing interest statement

The authors declare no conflict of interest.

Additional information

No additional information is available for this paper.

References

- [1] T. Magendran, S. Sanjeevi, Hyperion image analysis and linear spectral unmixing to evaluate the grades of iron ores in parts of Noamundi , Eastern India, *Int. J. Appl. Earth Obs. Geoinf.* 26 (2014) 413–426.
- [2] A.F.H. Goetz, V. Srivastava, Mineralogical mapping in the Cuprite mining district, Nevada, *J. Chem. Inf. Model.* 53 (9) (1985) 1689–1699.
- [3] R.N. Clark, Spectroscopy of rocks and minerals, and principles of spectroscopy, in: A.N. Rencz (Ed.), *Remote Sensing for the Earth Sciences*, 3, John Wiley and Sons, New York, 1999, pp. 3–58.
- [4] F. Kruse, “Mineral Mapping with AVIRIS and EO-1 Hyperion,” in *Summaries of the 12th Annual Jet Propulsion Laboratory Airborne Geoscience Workshop*, JPL Publication, Pasadena, California, Pasadena, 2003, pp. 149–156.
- [5] D. Ramakrishnan, R. Bharti, Hyperspectral remote sensing and geological applications, ” *Curr. Sci.*, 2015.
- [6] H. Govil, M.K. Tripathi, P. Diwan, Monika, Comparative evaluation of AVIRIS-NG and hyperion hyperspectral image for talc mineral identification. In *International Conferences on Data Management Analytics and Innovation*, 2019, pp. 95–101.
- [7] H. Govil, M. Kumar Tripathi, P. Diwan, S. Guha, Identification of Iron Oxides Minerals in Western Jahajpur Region, India Using AVIRIS-NG Hyperspectral Remote Sensing, 2018.
- [8] R.N. Clark, A.J. Gallagher, G.A. Swayze, USGS spectroscopy lab - spectral feature matching paper, in: *In Second Airborne Visible/Infrared Imaging Spectrometer (AVIRIS) Workshop*, 1990, pp. 176–186. JPL Publication 90-54.
- [9] F.D. van der Meer, et al., Multi- and hyperspectral geologic remote sensing: a review, *Int. J. Appl. Earth Obs. Geoinf.* 14 (1) (2012) 112–128.
- [10] C. Jing, Y. Bokun, W. Runsheng, T. Feng, Z. Yingjun, L. Dechang, Regional-scale mineral mapping using ASTER VNIR/SWIR data and validation of reflectance and mineral map products using airborne hyperspectral CASI/SASI data, *Int. J. Appl. Earth Obs. Geoinf.* 33 (2014) 127–141.
- [11] W.M. Baugh, F.A. Kruse, W.W. Atkinson, Quantitative geochemical mapping of ammonium minerals in the southern cedar Mountains, Nevada, using the airborne visible/infrared imaging spectrometer (AVIRIS), *Remote Sens. Environ.* 65 (3) (1998) 292–308.
- [12] A.P. Crósta, C. Sabine, J.V. Taranić, Hydrothermal alteration mapping at Bodie, California, using AVIRIS hyperspectral data, *Remote Sens. Environ.* 65 (3) (1998) 309–319.
- [13] F.A. Kruse, J.W. Boardman, J.F. Huntington, Comparison of airborne hyperspectral data and EO-1 Hyperion for mineral mapping, *IEEE Trans. Geosci. Remote Sens.* 41 (6) (2003) 1388–1400.
- [14] JPL NASA, ISRO - NASA AVIRIS – NG, Airborne Flights over India Sciene Plan Document for Hyperspectral Remote Sensing, 2015.
- [15] L. Hamlin, et al., Imaging spectrometer science measurements for terrestrial ecology: AVIRIS and new developments, *IEEE Aerosp. Conf. Proc.* August (2011).
- [16] A.K. Thorpe, et al., Mapping methane concentrations from a controlled release experiment using the next generation airborne visible/infrared imaging spectrometer (AVIRIS-NG), *Remote Sens. Environ.* 179 (2016) 104–115.
- [17] H. Govil, M. K. Tripathi, P. Diwan, and S. Guha, “Identification OF iron oxides minerals IN western jahajpur region , India using AVIRIS-NG hyperspectral remote sensing,” in *The International Archives of the Photogrammetry, Remote Sensing* and Spatial Information Sciences, Volume XLII-5, 2018 ISPRS TC V Mid-term Symposium “Geospatial Technology – Pixel to People”, 20–23 November 2018, Dehradun, India, 2018, vol. XLII, no. November, pp. 20–23.
- [18] M.K. Pandit, A.N. Sial, G. Malhotra, L.S. Shekhawat, V.P. Ferreira, C, O-isotope and whole-rock geochemistry of Proterozoic Jahazpur carbonates, NW Indian Craton, *Gondwana Res.* 6 (3) (2003) 513–522.
- [19] B. Dey, K. Das, N. Dasgupta, S. Bose, H. Ghatak, Zircon U-Pb SHRIMP dating of the Jahazpur granite and its implications on the stratigraphic status of the Hindoli-Jahazpur group, Seminar Abstract Volume, in: *Developments in Geosciences in the Past Deca*, 2016.
- [20] A.S.H.A. Saxena, M.K. Pandit, “Geochemistry of Hindoli group metasediments , SE aravalli craton , NW India: implications for palaeoweathering and provenance, *J. Geol. Soc. India* 79 (March) (2012) 267–278.
- [21] Geological Survey of India-District Report., “Geology and Minerals Resources of Bhilwara District, 1977.
- [23] T.V. King, R.N. Clark, in: F. Kuehn, T. King, B. Hoerig, D. Pieters (Eds.), *Verification of Remotely Sensed Data, Remote Sens. Site Charact*, Springer, Berlin, 2000, pp. 59–61.
- [24] I. SAC, Space application Center.pdf, SAC Cour. 41 (3) (2016).
- [25] S. Adler-Golden, A. Berk, L.S. Bernstein, S. Richtsmeier, P.K. Acharyal, M.W. Matthew, G.P. Anderson, C.L. Allred, L.S. Jeong, J.H. Chetwynd, Flaash, A Modtran4 Atmospheric Correction Package, 1994.
- [26] FLAASH User 's Guide, FLAASH User 'S Guide, 2005.
- [27] A.A. Green, M. Berman, P. Switzer, M.D. Craig, A transformation for ordering multispectral data in terms of image quality with implications for noise removal, *IEEE Trans. Geosci. Remote Sens.* 26 (1) (1988) 65–74.
- [28] K. Singh, K. Rajaprian, M. Vinothkumar, R.S. Kumar, “Hyperspectral remote sensing approach for lithological discrimination by ASTER data – a case study of thenkalmalai and odhimalai hills, tamilnadu, India, *Int. J. Adv. Earth Sci. Eng.* 2 (1) (2013) 75–83.
- [29] K. Pazand, J.F. Sarvestani, Hydrothermal alteration mapping using ASTER data for reconnaissance porphyry copper mineralization in the ahar area , NW Iran, *Indian Soc. Remote Sens.* 41 (June) (2013) 379–389.
- [30] F.D. Van Der Meer, et al., “International journal of applied earth observation and geoinformation multi- and hyperspectral geologic remote sensing: a review, *Int. J. Appl. Earth Obs. Geoinf.* 14 (1) (2012) 112–128.
- [31] ENVI USER GUIDE, “ENVI User ' S Guide, 2004.
- [32] J.W. Boardman, F.A. Kruse, Analysis of imaging spectrometer data using N-dimensional geometry and a mixture-tuned matched filtering approach, *IEEE Trans. Geosci. Remote Sens.* 49 (11) (2011) 4138–4152.
- [33] J.W. Boardman, F.A. Kruse, R.O. Green, “Mapping target signatures via partial unmixing of aviris data,” *Jet propuls. Lab* 23 (1995) 23–26.
- [34] A.H. El-Nahry, U. Altinbas, Processing and analyzing advanced hyperspectral imagery data for identifying clay minerals . A case study, *J. Appl. Sci. Res.* 2 (4) (2006) 232–238.
- [35] F.A. Kruse, et al., “The Spectral Image Processing System (SIPS)—interactive visualization and analysis of imaging spectrometer Data, *Remote Sens. Environ.* 44 (1993) 145–163.
- [36] F.A. Kruse, A.B. Lefkoff, J.B. Dietz, Expert system-based mineral mapping in northern death valley, California/Nevada, using the airborne visible/infrared imaging spectrometer (AVIRIS), *Remote Sens. Environ.* 44 (2–3) (1993) 309–336.
- [37] D.A. Dennison, P.E. Roberts, Endmember selection for multiple endmember spectral mixture analysis using endmember average RMSE, *Remote Sens. Environ.* 87 (2003) 123–135.
- [38] P.E. Dennison, K.Q. Halligan, D.A. Roberts, A comparison of error metrics and constraints for multiple endmember spectral mixture analysis and spectral angle mapper, *Remote Sens. Environ.* 93 (2004) 359–367.
- [39] F. Van der Meer, Analysis of spectral absorption features in hyperspectral imagery, *Int. J. Appl. Earth Obs. Geoinf.* 5 (1) (2004) 55–68.
- [40] Harris Harris, Geospatial solutions, in: *Continuum Removal*, 2017. Retrieved. (Accessed 10 June 2017).
- [41] F.D. Van der Meer, P. Van Dijk, H. Van der Werff, H. Yang, Remote sensing and petroleum seepage: a review and case study, *Terra. Nova* 14 (2002) 1–17.
- [42] C. Roberto, D.E.S. Filho, Hyperspectral remote sensig for mineral mapping: a case study at: a case -study at Alto Paraiso de Goias, Central Brazil, *Rev. Bras. Geociencias* 30 (3) (2000) 551–554.